Annales Geophysicae, 23, 2095–2105, 2005
SRef-ID: 1432-0576/ag/2005-23-2095

Annales Geophysicae

E-region wind-driven electrical coupling of patchy sporadic-E and spread-F at midlatitude

S. Shalimov[1] **and C. Haldoupis**[2]

[1]Institute of the Physics of the Earth, Moscow, Russia
[2]Physics Department, University of Crete, Iraklion, Greece

Received: 11 August 2004 – Revised: 14 March 2005 – Accepted: 20 June 2005 – Published: 15 September 2005

Abstract. This paper investigates the role of neutral winds in the generation of relatively large polarization electric fields across patchy sporadic-E layers, which then map upward to the F region, to create conditions for medium-scale spread-F. The calculations are based on an analytical model that uses the current continuity equation and field-aligned current closures to the F region in order to describe quantitatively a Hall polarization process inside sporadic-E plasma patches during nighttime. In applying this model we use experimentally known values for E and F region, conductances, the ambient electric fields and prevailing neutral winds, in order to estimate the polarization fields that build up inside sporadic-E. It is found that the relatively strong west-southwest neutral winds during summer nighttime can provide the free energy for the generation of sizable polarization electric fields, which have comparable eastward and north-upward components and reach values of several mV/m. Given that the sporadic-E patches have sizes from a few to several tens of kilometers, the polarization fields can map easily to the F region bottomside where they impact $\boldsymbol{E}\times\boldsymbol{B}$ plasma uplifts and westward bulk motions, in line with key observational properties of medium-scale spread-F. However, the present simple model needs further development to also include wind forcing of the F region plasma and possible polarization processes inside spread-F.

Keywords. Ionosphere (Electric fields and currents; Ionospheric irregularities; Mid-latitude ionosphere)

1 Introduction

In the summer nighttime, the midlatitude ionosphere is dominated by the presence of sporadic-E layers (E_s) in the E region and spread-F (SF) structures in the F region. Both phenomena are clearly identifiable in the ionograms which have been used for their study over many years. Although observations have existed for a long time in favor of a relationship between midlatitude E_s and SF (e.g. see Bowman, 1985), the study of sporadic-E and spread-F evolved rather independently. Recently, however, and as a result of new knowledge on sporadic-E and because of concurrent SF and E_s plasma density measurements made with the incoherent scatter radar (ISR) at Arecibo, the study of the sporadic-E – spread-F relation has attracted attention and renewed interest. Naturally, the reason behind the E_s–SF connection lies in the electrical coupling of E and F regions via the magnetic field lines, considered in the framework of dynamics and electrodynamics of the coupled thermosphere-ionosphere system.

Recently, two companion papers by Kelley et al. (2003) and Haldoupis et al. (2003) provided supporting evidence and proposed a new mechanism on the role of patchy sporadic-E layers in forming medium scale spread-F at midlatitude. In this mechanism, enhanced electric fields inside sporadic-E patches can map along the magnetic field lines up to the F region, to uplift the plasma and generate spread-F. In this process, the nighttime F region acts as the electrical load on a generator forming inside the sporadic-E layer plasma. A somewhat similar scenario on coupled electrodynamics in the midlatitude ionosphere has also been proposed by Tsunoda and Cosgrove (2001).

With respect to the elevated electric fields inside sporadic-E, these are attributed to a Hall-current polarization process which can sustain polarization fields an order of magnitude higher than the ambient F region dynamo fields during nighttime. This Hall polarization process was introduced by Haldoupis et al. (1996, 1997), in order to account for the large electric fields required for the excitation at midlatitude of the modified two stream, or Farley-Buneman instability. This instability was detected first at midlatitude by the Sporadic-E Scatter experiment (SESCAT) in Greece and reported by Schlegel and Haldoupis (1994). The magnitude of the polarization fields inside E_s depends on the driving ambient electric field and the current-closure system coupling to the F region via field-aligned currents, which also implicates a

Correspondence to: S. Shalimov
(pmsk4@mail.ru)

role for the E and F region Pedersen conductances and the E_s patch dimensions. The problem of current-closure in the F region was treated analytically by Shalimov et al. (1998) and numerically by Hysell and Burcham (2000), Hysell et al. (2002), and more recently by Yokoyama et al. (2003, 2004).

The present paper comes as a continuation of our recent work reported by Haldoupis et al. (2003) and Kelley et al. (2003), which are referred to in the following as paper A and B, respectively. The idea here is to apply the analytical current closure model of Shalimov et al. (1998), after it is modified to also include wind-induced $\boldsymbol{U}\times\boldsymbol{B}$ fields, in order to explore in a quantitative fashion the proposed mechanism of electrical E_s-SF coupling. In order for the calculations to be as realistic as possible we use observational facts to define key parameters of the model and thus test its applicability and assess its predictions. In particular, the paper looks into the effects of the prevailing E region neutral winds during strongly unstable sporadic-E conditions. These winds are now recognized as the main source of free energy that drives the Hall polarization process inside E_s which can destabilize the E_s plasma, and lead also to spread-F in accord with the mechanism proposed in A and B.

In the following, key experimental properties are summarized for both the unstable sporadic-E and spread-F, and then the mechanism proposed for spread-F generation is outlined. Next, the field-aligned current closure model that estimates the zonal and meridional polarization fields inside a sporadic-E patch is presented and then applied to obtain numerical estimates which quantify the conditions necessary for spread-F generation. Finally, the paper closes with a summary, concluding comments, and remaining problems.

2 Key observational properties

Papers A and B provided experimental evidence for a connection between spread-F and unstable sporadic-E. The term "unstable" here means that the electric fields inside E_s are enhanced and thus allow for the excitation of the gradient drift and/or the modified two stream plasma instabilities. In other words, unstable E_s means that these layers can be detected with coherent backscatter radars pointing perpendicular to the Earth's magnetic field. In the following we summarize key observational facts relating to unstable sporadic-E and spread-F at midlatitude. For details, see papers A and B and also many references therein, some of them also quoted below.

2.1 Unstable sporadic-E

The unstable sporadic-E has been studied over the last 15 years mostly with midlatitude backscatter radars (e.g. Yammamoto et al., 1992; Haldoupis and Schlegel, 1993; Hysell and Burcham, 2000; among many others), but also with rockets (e.g. Fukao et al., 1998, and more papers in the same Geophys. Res. Lett. issue), as well as ionosondes and incoherent scatter radars (e.g. Riggin et al., 1986; Hussey et al., 1998; Ogawa et al., 2002; Hysell et al., 2004). The following is a list of observational characteristics of unstable E_s, which are of interest to the present study:

1. The unstable E_s is a summer nighttime phenomenon occurring mostly prior to 02 LT and relating to spread E_s, that is, corrugated and patchy sporadic-E.

2. The observed Doppler velocities are mostly negative, corresponding to northward and upward irregularity velocities; they usually take values less than 150 m/s but also at times are well above this limit, exceeding even the ion acoustic speed threshold for the Farley-Buneman instability. The Doppler velocities are attributed to $\boldsymbol{E}\times\boldsymbol{B}$ motions which implies the presence of enhanced eastward electric fields of several millivolts per meter, that is, well above the ambient dynamo fields at midlatitude.

3. Studies with the Valensole radar in the south of France, which was the only midlatitude radar capable of monitoring a large azimuthal sector (e.g. see Bourdillon et al., 1995; Haldoupis et al., 2001), showed that E_s backscatter relates to plasma structures, presumably patches of sporadic-E that drift across the radar field-of-view, mostly westwards. On the average, the zonal scale lengths of the unstable patches extend from a few tens to several tens of kilometers, say, between 20 and 100 km.

4. The E_s backscattered power often undergoes strong quasi-periodicities (QP echoes) with periods ranging from a few minutes to more than an hour. The QP echoes are attributed to unstable E_s patches which drift with the wind and thus form sequential sloping striations in the range-time-intensity (RTI) plots, having mostly negative range rates dR/dt that take values from about 20 to 80 m/s. Since most radars observe northwards, these speeds are attributed to southward neutral winds.

5. Beam forming radars, including the Middle and Upper atmosphere (MU) radar in Japan and the Valensole radar in southern France, as well as several radio interferometer studies show, that the E_s patches move predominantly westward with the neutral wind, with speeds ranging from 30 to 150 m/s, and sometimes even higher. Such large E region westward neutral winds were also inferred from many chemical release wind measurements (e.g. see Larsen, 2002).

2.2 Spread-F at medium scale

The midlatitude "spread-F" dealt with in this paper refers to F region plasma structures with intermediate scale sizes, that is, having azimuthal extents ranging from a few tens to many tens of kilometers. Our knowledge of this type of spread-F

is based on several studies, including the early ISR measurements at Arecibo by Behnke (1979), the MU F region coherent radar studies in Japan by Fukao et al. (1991), the all-sky airglow imaging and ISR measurements in Arecibo by Mendillo et al. (1997), and a joint coherent–incoherent radar study in Arecibo by Swartz et al. (2002). The key properties of this phenomenon which are of interest to the present study are summarized as follows:

1. Spread-F occurs mainly in the summertime, always during dark hours, (e.g. see statistics presented recently by Shiokawa et al. (2003)).

2. Spread-F is identified with ionospheric regions of electron density depletions because of abrupt plasma uplifts. The F region uplifts are attributed to upward and northward plasma upwelling. The observed upwelling velocities are mostly between 50 and 200 m/s but at times can exceed 300 m/s. The measured uplifts range in height from about 20 km to 80 km.

3. The MU radar measurements show the uplifted regions to move westward with speeds exceeding 100 m/s, whereas the airglow imagers measured west-southward motions with speeds ranging from 50 to 120 m/s.

4. The Arecibo ISR and MU radar observations suggest azimuthal scale sizes less than 100 km, whereas the airglow imagers indicate much larger scale regions of depleted plasma between 100 and 500 km. It is not yet clear, however, if these two observations are directly related, in view also of a recent result published by Shiokawa et al. (2003) which shows poor correlation between large-scale airglow bands of depleted plasma and classic spread-F measured with ionosondes.

3 A new mechanism for spread-F generation

For completeness, we describe here, in brief, the mechanism for intermediate scale spread-F generation at midlatitude, proposed recently by Kelley et al. (2003) and Haldoupis et al. (2003). The process is outlined in Fig. 1, which is nearly the same as Fig. 4 in the paper by Haldoupis et al. (2003). Shown are highly conducting sequential sporadic-E plasma patches embedded in the weakly conducting nighttime E region. The E_s patches have finite extent in both the zonal (east-west) and meridional (south-north) directions, and drift with the prevailing neutral wind $\boldsymbol{U}$ which is directed west-southward. If $\hat{x}$ is horizontal to the east, $\hat{y}$ southward and downward and $\hat{z}$ is along the magnetic field, then in this configuration an ambient electric field $\boldsymbol{E}_0+\boldsymbol{U}\times\boldsymbol{B}$ could generate a fairly large polarization field $\boldsymbol{E}^p$ pointing in the north-east quadrant, in line with the Hall polarization process of Haldoupis et al. (1997). At steady state, the polarization field adjusts itself so that divergence-free current flow is established inside the patch through field-aligned current closures in the F region.

With respect to spread-F generation, it is postulated that the polarization electric fields inside the sporadic-E patches can map along the field lines up to F region altitudes. As shown in Fig. 1, large eastward fields can act upon the magnetized F region plasma to impact northward and upward $\boldsymbol{E}\times\boldsymbol{B}$ drifts of both the electrons and ions, causing F region plasma uplifts and therefore spread-F. On the other hand, the northward and upward polarization field $\boldsymbol{E}_y^p$ can also cause westward plasma drifts and thus account for the westward motions of spread-F, as reported, for example, by Fukao et al. (1991). Finally, as seen in Fig. 1, a westward electric field can also be established inside the low conductivity space between patches because the neighboring edges are oppositely charged. These fields may also map at times in the F region and thus drive downward and southward $\boldsymbol{E}\times\boldsymbol{B}$ plasma drifts at the uplifted region boundaries, very much in line with the observations of Fukao et al. (1991).

As concluded in papers A and B, the proposed mechanism seems to be capable of qualitatively explaining some key experimental properties of medium scale spread-F and thus account for at least some forms of midlatitude spread-F. In the following we test the validity and feasibility of this mechanism in a more rigorous way by applying the model of Shalimov et al. (1998) for the case of a sporadic-E plasma patch that drifts horizontally with the neutral wind.

4 A wind-driven polarization model inside E_s

The Hall polarization process inside a sporadic-E plasma patch has been treated analytically by Shalimov et al. (1998), who used a three-dimensional model of divergence-free current flow. The model assumes a weak ambient dynamo electric field which causes polarization charges to built up in both the east-west and north-south patch boundaries, so that at steady state a divergence free current flow, $\nabla\cdot\boldsymbol{J}=0$, is established through zonal and meridional field-aligned current closures. It was found that the polarization process can become effective for elongated E_s patches under the action of an enhanced ambient electric field that initiates the process. Here we postulate that the large driving electric fields necessary for the polarization process to become effective are dynamo fields provided by the strong neutral winds which are known to exist during unstable E_s conditions.

In their analysis, which is now updated for the purpose of completeness in the Appendix, Shalimov et al. (1998) used a non-orthogonal coordinate system with the z-axis pointing along $\boldsymbol{B}$ and forming a magnetic dip angle I with the horizontal; the y-axis was taken to be horizontal in the meridional plane and positive southward, whereas the x-axis was perpendicular to both $\hat{y}$ and $\hat{z}$ and pointing eastward. Under the action of an ambient $\boldsymbol{E}$ field the following set of equations were obtained for the zonal and meridional polarization fields inside the plasma patch (see details in the Appendix):

$$E_x + E_x^p - \frac{R}{S}(E_y - E_y^p) = -E_x^p Z S^2 (1/S^2 L^2 + 1) \qquad (1)$$

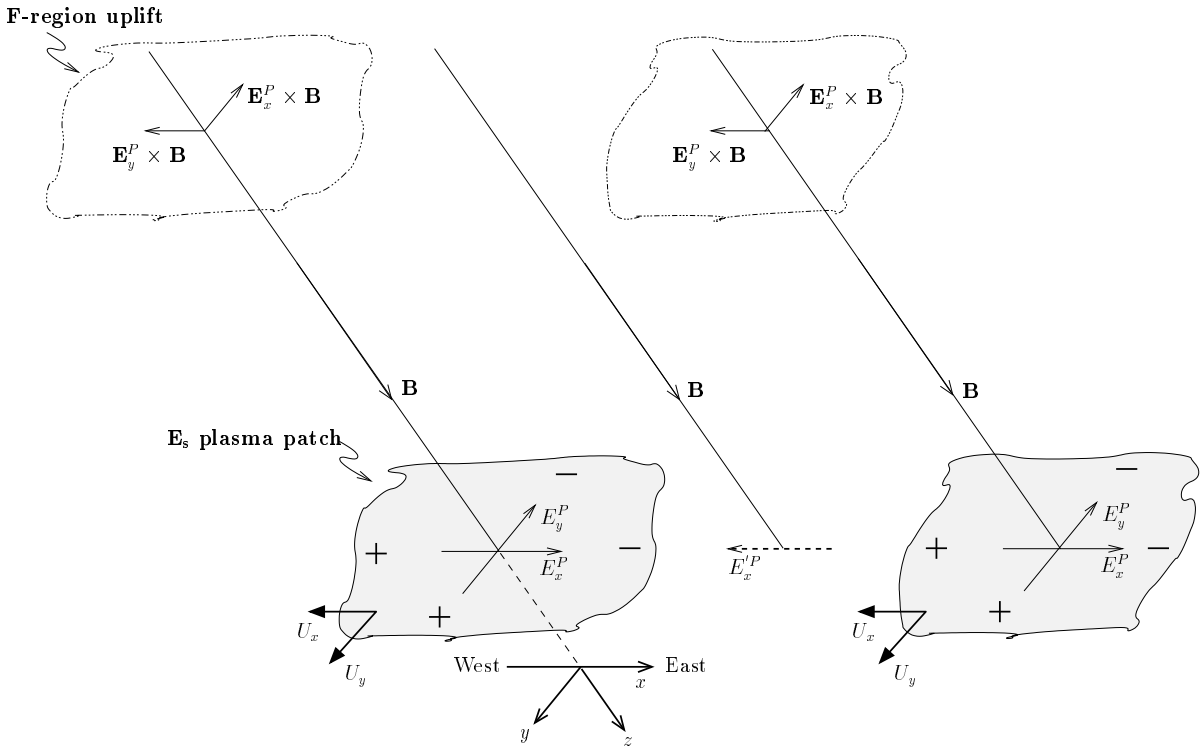

Fig. 1. Schematic illustrating the electrical coupling between sporadic-E patches and the F region which can lead to spread-F generation. Under the action of a west-south wind the sporadic-E patches become polarized and a polarization electric field builds up pointing into the north-east quadrant. This field maps to the F region bottomside where it causes $\boldsymbol{E}\times\boldsymbol{B}$ plasma uplifts and westward drifts.

$$\frac{R}{S}(E_x+E_x^p)+\frac{(E_y-E_y^p)}{S^2}=E_y^p Z S^2 L^2(1/S^2L^2+1), \qquad (2)$$

where E_x^p, E_y^p are the eastward and northward components of the polarization electric field, respectively, $S=\sin I$, $C=\cos I$, $L=l_y/l_x$ is the meridional to zonal patch extent ratio, $R=\Sigma_H^s/\Sigma_P^s$ is the Hall to Pedersen conductance ratio inside E_s, and $Z=\Sigma_P/\Sigma_P^s$ with Σ_P being the Pedersen conductivity integrated along the magnetic field lines from above E_s through the F region. In order to obtain Eqs. (1) and (2) it was assumed that $l_x/l_\parallel<1$, $l_y/l_\parallel<1$, where $l_\parallel\approx\sqrt{\sigma_0/\sigma_P}/\sqrt{1/l_x^2+1/S^2l_y^2}$ is the mapping length in accordance with the electric field mapping theory of Farley (1959).

If the ambient electric field includes a wind induced $\boldsymbol{U}\times\boldsymbol{B}$ field as well, then in the last equations the driving electric field components become

$$E_x = E_x^0 + U_y B S^2, \qquad E_y = E_y^0 - U_x B, \qquad (3)$$

so that the action of the neutral wind on the sporadic-E polarization process is also taken into account. At steady state, the combined forcing of the ambient dynamo fields and the meridional and zonal winds on the sporadic-E patch will adjust the zonal and meridional polarization fields accordingly, also through field-aligned current closures.

By following the procedure described in detail by Shalimov et al. (1998), one can solve the Eqs. (1) and (2) for E_x^p and E_y^p to obtain

$$E_x^p = \frac{-E_x A + E_y B}{D}, \qquad E_y^p = \frac{E_x B + E_y C}{D}, \qquad (4)$$

where $Z_1=ZS^2(S^{-2}+L^2)$, $A=(Z_1S^2+R^2+1)$, $B=SRZ_1$, $C=(Z_1L^{-2}+R^2+1)$, $D=R^2+(1+Z_1L^{-2})(1+Z_1S^2)$, where also $E_{x,y}$ are defined by Eq. (3). The last two expressions will be used in the following section to obtain numerical results and thus investigate the conditions necessary for the E_s–SF electrical coupling to become effective.

Shalimov et al. (1998) have shown that the polarization process depends strongly on the Pedersen conductance ratio Z, inside and above the layer and the driving electric field. In addition, this mechanism is more effective if dense sporadic-E layer patches are elongated in the north-south direction in order for the east-west polarization electric field to set up, and vice versa. The elongation follows from the need that the field-aligned current closure loop, through which the current along the elongated patch closes through the magnetic field lines in the F region, reduces drastically a secondary polarization field to build up which can counteract the primary polarization field. In essence, the last point originates from the well known Farley's (1959) theory on electric field mapping along the field lines in the ionosphere.

Since the analytical model of Shalimov et al. (1998), there were several more papers that dealt with the problem of large polarization fields inside sporadic-E plasma patches, using both analytical and numerical models. All these papers assessed the results of the Shalimov et al. theory rather positively and confirmed several of its predictions. Hysell and Burcham (2000) used a numerical model to show that large polarization electric fields can be generated by elongated patchy sporadic-E layers electrically coupled to the F region dynamo. In their computations, however, they used absolute scales for the transverse sizes of the plasma patch and did not consider Pedersen conductance effects inside and above the layer. Cosgrove and Tsunoda, in a series of papers which are summarized and listed in a recent review paper by Tsunoda et al. (2004), considered an alternative option of current closures within the layer itself, although later also added effects of F region conductivities. Hysell et al. (2002) advanced their previous simulations to obtain time dependent results that revealed a much more complicated picture than the analytical model predicted, and showed that plasma patches tend also to become unstable to kilometer scale plasma waves. Finally, in a series of two papers, Yokoyama et al. (2003, 2004) published 2-D and 3-D simulations of polarization electric fields inside sporadic-E clouds driven also by neutral winds and using current closures either inside the layer and/or in the F region. Among the several features revealed in their simulations, the importance of both, the patch elongation and the Pedersen conductance ratio inside and outside sporadic-E, in line with the predictions of the Shalimov et al. (1998) analytical model was also recognized.

5 Numerical results

In order to compute from the last two equations the polarization field components E_x^p and E_y^p inside the E_s plasma patch, we need to choose representative values for the various parameters in Eqs. (1) and (2). Starting from the Hall to Pedersen conductance ratio R inside the layer, we use R=12 which, as shown by Shalimov et al. (1998), is representative for a 3-km-thick sporadic-E layer centered near 105 km, with a peak electron density of 3×10^{11} m^{-3} and a large abundance of heavy metallic ions, leading to a mean ionic mass of about 44 amu. With respect to the layer horizontal extent ratio L, we do not use the rather unrealistic elongations inferred by Shalimov et al. (1998) and let L take values ranging between 0.2 to 5, that is, the patch zonal and meridional extents are chosen so not to be grossly different.

In order to use appropriate values for the F- to E-region Pedersen conductance ratio $Z=\Sigma_P/\Sigma_P^s$, we rely on existing measurements. Harper and Walker (1977) used Arecibo ISR observations in the summer nighttime during solar minimum to find that Z can differ from night to night, taking values between 1.0 and 10.0, depending on the occurrence of sporadic-E and the degree of variability in the F region. On the other hand, Swartz et al. (2002) estimated the F to E region conductance ratio to be near 5 or greater during normal conditions but drops to almost 1.5 during times when a strongly uplifted F layer above and an intense sporadic-E layer below occurred concurrently. Also, in the two spread-F events studied by Kelley et al. (2003), the ratio of F to E-layer height integrated Pedersen conductivities was estimated to be in the range from 1.5 to 10. Given all this, we take $1<Z<10$.

Finally, with respect to the driving E region winds, we have taken into consideration the experimental findings summarized in Sect. 2 showing prevailing westward winds from 50 to 150 m/s and southward winds from 20 to 80 m/s during unstable E_s conditions. Note that a 100-m/s neutral wind can induce at midlatitude an electric field of about 4 to 5 mV/m, which is quite stronger than the mean ambient dynamo field. The latter is pointing into the southeast quadrant and has comparable zonal and meridional components near 1 mV/m, in accord with what is observed at midlatitude for the pre-midnight sector during summer (e.g. see Kelley, 1989). In the Hall polarization process under consideration, a westward (southward) wind will induce a southward $\boldsymbol{U}_x\times\boldsymbol{B}$ (eastward $\boldsymbol{U}_y\times\boldsymbol{B}$) electric field which can set up an eastward (north-upward) polarization electric field at the E_s patch boundaries.

In order to interpret the predictions of the model, one needs to consider that the eastward polarization field drives a northward and upward electron Hall current inside E_s, which then reinforces the polarization field caused by the southward wind. On the other hand, the north-upward field counteracts to and thus reduces, the eastward polarization field because it tends to drive a secondary electron Hall current to the west.

Figure 2 presents estimates of eastward (top panel) and north-upward (bottom panel) polarization electric fields inside a sporadic-E plasma patch. The calculations are made by using Eq. (4) for a magnetic dip I=53° and typical westward and southward winds of 100 m/s and 40 m/s, respectively. Given that the ambient $\boldsymbol{E}_x^0$ and $\boldsymbol{E}_y^0$ field components are 1 mV/m, the effective driving fields are about 5.5 mV/m and 2.5 mV/m for the south and eastward components, respectively. Then the estimated polarization electric fields at steady state are plotted in Fig. 2, as a function of the F to E region conductance ratio Z and the meridional to zonal extent ratio L of the sporadic-E plasma patch.

Inspection of the top panel in Fig. 2 shows the generation of fairly strong eastward polarization fields ranging between 5 and 10 mV/m and becoming larger for larger ratios L, that is, when the patch is elongated in the meridional direction. The strength of E_x^p is relatively insensitive to the conductance ratio Z, a fact that is anticipated for low Z, whereas for a relatively large Z it is somewhat counterintuitive. This is understood, however, because large Z reinforces enhanced current flows between E_s and F regions under strongly driven conditions. This means that both the Hall current inside the patch and the field-aligned current between E and F regions become larger than when Z is small, which, in turn, leads to a larger E_x^p. This conclusion agrees with both the analytical results of Shalimov et al. (1998) and the numerical findings of Yokoyama et al. (2004).

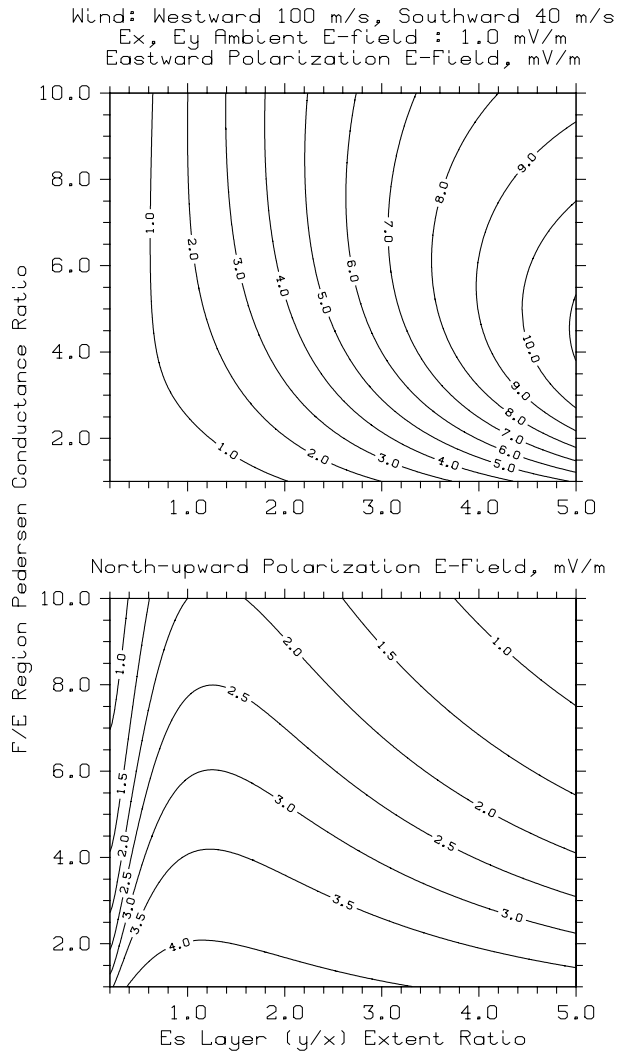

Fig. 2. Model predictions for the eastward (upper panel) and north-upward (lower panel) polarization fields inside a sporadic-E patch, as a function of the meridional to zonal patch extent ratio and the F to E region conductance ratio. The model predictions are for typical E region winds during unstable sporadic-E conditions, that is, with the wind having a westward component of 100 m/s and a southward component of 40 m/s. See text for more details.

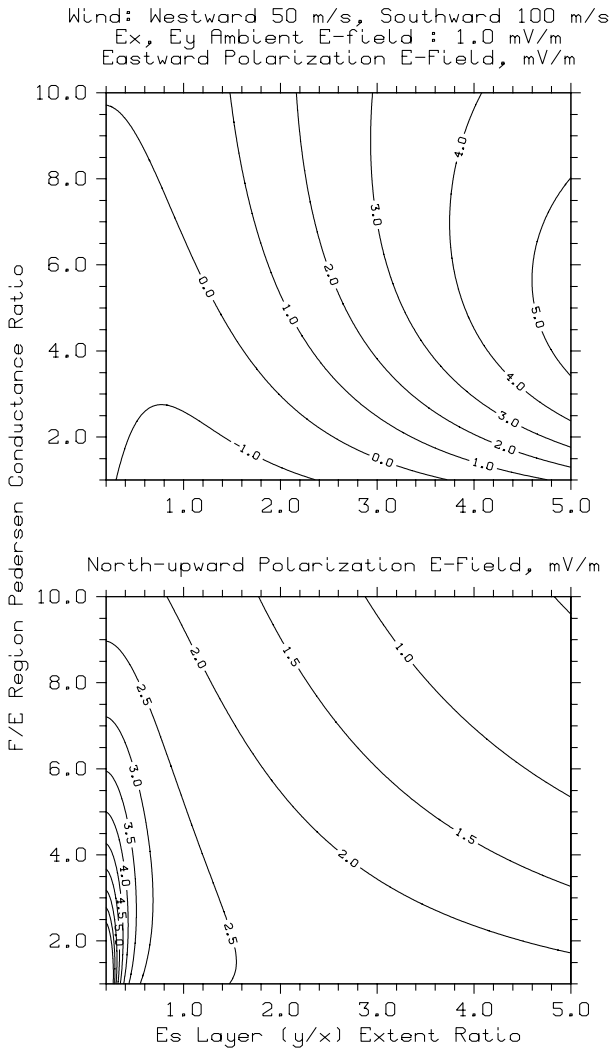

Fig. 3. Same as Fig. 2 but for the case of a strong southward wind component (100 m/s) that is larger than the westward wind component (50 m/s). In this case, the situation reverses relative to the one in Fig. 2 and we can have large meridional polarization fields if the patch is relatively elongated in the zonal direction.

On the other hand, at small L the eastward field becomes fairly weak because of the counteracting role of the north-upward polarization field which, as shown in the bottom panel, becomes stronger with smaller L. Figure 2 shows that the strongest northward and upward polarization fields range from about 3.0 to 4.0 mV/m for relatively small ratios Z, that is, for $Z<5$, and low L ratios. This can be understood from Eq. (2), and it is discussed in detail by Shalimov et al. (1998). For example, if the F region Pedersen conductance decreases because of an ongoing uplift of plasma, this will reduce the electrical load on the E region generator and lead to a smaller eastward polarization field. At first look this seems unexpected, but it happens because at relatively small Z the north-upward field E_y^p does become stronger and thus producing a counteracting effect to reduce the eastward Hall polarization current that sets up E_x^p.

In summary, for strongly driven wind conditions, that is, for a strong westward and a weaker southward wind, as in Fig. 2, there is a combination of L and Z that allows both components of the polarization field to take up enhanced values. These fields can map to the F region, impacting $\boldsymbol{E}\times\boldsymbol{B}$ plasma uplifts and westward drifts and thus generate spread-F.

Finally, we also consider the case when the southward driving wind is larger than the westward wind. This is illustrated in Fig. 3 which is the same as Fig. 2 but here we apply a westward wind of 50 m/s and a southward wind of 100 m/s. Contrary to Fig. 2 the eastward polarization field (upper panel) is now weak, not only because the driving westward wind is half of that used before but also because

of the counteracting effects of the applied large southward wind. This can reduce E_x^p considerably for any L, and even can reverse its polarity for small L, that is, for a zonally elongated plasma patch, as seen in the lower left corner of the upper panel. In this case, the model predicts a large north-upward polarization field which can map to the F region and cause large westward plasma drifts. On the other hand, there will be no eastward polarization field acting upon the F region plasma; therefore, we conclude that the situation in Fig. 3 cannot lead to F region uplifts, but it may cause downward and south-westward bulk motions of F region plasma.

6 Polarization field mapping

Here we discuss briefly the mapping efficiency of the E_s-patch polarization fields along the magnetic field lines to the F region. The theory of Farley (1959) shows that the electric field mapping is determined by the ratio $\sqrt{\sigma_0/\sigma_P}$, where σ_0 is the conductivity parallel to the magnetic field and σ_P is the Pedersen conductivity at the altitude where the current loop closes. This means that the field mapping from the E to the F region is more effective if the F region Pedersen conductivities are lower rather than higher. The mapping ratio $\sqrt{\sigma_0/\sigma_P}$ is approximately 60 near 100 km and 1000 at 300 km (e.g. see Kelley, 1989).

With respect to the mapping efficiency, the theories of Farley (1959) and LaBelle (1985) show that this can be estimated from the term e^{-kl}, where l is the distance along the magnetic field lines for the electric field to be mapped, and k is an effective wave number which relates to the size of the structure perpendicular to $\boldsymbol{B}$ where the electric field is generated. For the Shalimov et al. (1998) model, $k \sim 1/l_\parallel$, where

$$l_\parallel \sim \sqrt{\sigma_0/\sigma_P}/\sqrt{1/l_x^2 + 1/S^2 l_y^2}. \quad (5)$$

Using the last expression, one can estimate that for the E_s patches under consideration, that is, with characteristic horizontal extents ranging from about 20 to 100 km (e.g. see Sect. 2.1), the mapping of the polarization field to the F region becomes fairly effective. For example, using a conservative value of 200 for $\sqrt{\sigma_0/\sigma_P}$ we obtain a mapping efficiency at 300 km of about 95% and 99% for horizontal scale lengths $l_x \sim l_y$ equal to 20 km and 100 km, respectively. Given that l_x, l_y range from a few tens to several tens of kilometers, we conclude that the mapping of the polarization electric fields from the E_s plasma patch to the F region is done with little attenuation.

7 Summary and discussion

In this paper we applied an extended version of the analytical current closure model developed by Shalimov et al. (1998), in order to investigate quantitatively the electrical coupling between unstable sporadic-E layers and the F region, which can lead to spread-F generation. The effects of the prevailing E region neutral winds acting as a source of free energy upon sporadic-E plasma patches were considered. Note that, the $\boldsymbol{E}$ region winds, which appear to be rather large around 105 km, are now recognized more and more as the main drivers of the Hall polarization process inside patchy E_s (e.g. see Tsunoda et al., 2004; Yokoyama et al., 2004). We show here that these large winds can generate enhanced polarization electric fields inside patchy E_s which then map along the magnetic field lines upward to distort the F region bottomside.

The following scenario of coupled $E_s - SF$ electrodynamics, based on the E region Hall polarization process, can be drawn. A sporadic-E plasma patch is imbedded in the weakly conducting low electron density nighttime E region, with a neutral wind pointing into the west-southwest sector and a small south-east electric field imposed by the F region dynamo to represent a typical situation. In this configuration, and under the action of the wind-induced and ambient electric fields, polarization fields are set up across the patch boundaries as a result of divergence-free current flow inside the patch through field-aligned current closures in the F region. The field-aligned current closures are an essential component of the system because in their absence the E region polarization process cannot maintain large electric fields across the patch. We have shown in this paper that the magnitude of the zonal and meridional polarization fields depends mainly on the driving winds but also on several quantities which include the Hall to Pedersen conductance ratio R inside E_s, the F to E region Pedersen conductance ratio Z, and the patch meridional to zonal extent ratio L.

The model shows that for common conditions, when the E_s patch drifts with a sizable westward wind ($\sim$100–120 m/s) and a smaller southward wind ($\sim 40-50$ m/s), strong eastward polarization electric fields (greater than 4 to 6 mV/m) can be generated for Z=6–10 and moderate meridional patch elongations of L=2–3; at the same time, a weaker upward and northward polarization field can also be established. Larger eastward fields can exist for smaller F to E region conductance ratios, that is, for $Z \sim$1–2, if the plasma patch becomes elongated along the north-south direction (L=3–5). In this case the zonal and meridional polarization electric fields may become comparable.

The present model predicts that the eastward and northward polarization field components can reach fairly elevated values inside the patch relative to the ambient mean dynamo fields during nighttime. Since we deal here with medium scale sporadic-E patches, that is, patches having horizontal scale lengths ranging from a few tens to several tens of kilometers, the polarization fields can map easily to the F region bottomside and therefore impact $\boldsymbol{E} \times \boldsymbol{B}$ plasma motions there. The eastward polarization field will quickly uplift the F region plasma, whereas the north-upward polarization field will push the plasma westward. This situation can lead to spread-F generation and thus account for key observations of spread-F at mesoscale.

As discussed in the papers by Kelley et al. (2003) and Haldoupis et al. (2003), an eastward polarization electric field of 5 mV/m inside a medium-scale E_s patch will map instantly

up along the field lines to produce a 50-km uplift of the F region bottomside in about 10 min, whereas a 10-mV/m field will need only about 5 min for the same uplift. This process will be much more effective if both the sporadic-E patch below and the uplifted plasma region above are somehow kept "in contact", by moving horizontally with comparable velocities. This actually has been observed to take place in the simultaneous sporadic-E and spread-F observations of Swartz et al. (2002), made with the Arecibo incoherent scatter radar. Furthermore, the unstable sporadic-E layers are known to move overwhelmingly westward, a fact that compares well with observed westward bulk motions of uplifted spread-F structures, as reported, for example, by Fukao et al. (1991). The present model, which predicts sizable northward and upward polarization electric fields, can account for the westward $\boldsymbol{E}\times\boldsymbol{B}$ motions of spread-F, which are needed in order for the spread-F structures to "escort" the E_s patches in their westward drift with the neutral wind.

However, in addition to the dominant E_s–SF westward motions just mentioned, one has to consider that the unstable sporadic-E patches undergo a smaller southward motion with the neutral wind. Therefore, in order for an uplifted F region volumes to be able to track the wind-drifting E_s patches below, they must also be subject to a southward motion. It is likely that such southward motions of spread-F do exist because they have been measured often with airglow imagers (e.g. see Garcia et al. (2000) and more references therein).

Our present model, which relies on an eastward polarization field for an F region plasma uplift to occur, cannot account for a southward F region plasma drift because the eastward polarization field drives the plasma northward rather than southward. Obviously, this is a discrepancy of the present model which requires attention and investigation. One possible way out is to consider in addition to the electric field effects, the meridional neutral wind forcing of the F region plasma. For example, the combination of an eastward electric field, which is provided by the E_s generator below, and a southward wind in the F region may be so that the counteracting wind effect reverses the northward $E_x^p B\sin I$ motions, while at the same time it reinforces the plasma uplift. Although this option requires more consideration, it may be at work also in view of the fact that the mean neutral wind in the nighttime F region has a dominant southward component (e.g. see Kelley and Makela, 2001). Alternatively, the polarization state of the uplifted F region structure may also be of importance (e.g. see again Kelley and Makela, 2001), a topic which was not considered in the present model.

We conclude that the details of the electrodynamic coupling between patchy the sporadic-E and F region requires more study. In particular, we need to have carefully designed multi-sensor experiments using the incoherent scatter radar facility in Arecibo as the basic instrument.

Appendix A

As in the paper by Shalimov et al. (1998), a nonorthogonal coordinate system with the z axis pointing along the geomagnetic field was used to form an angle with the horizontal that equals the magnetic dip angle I. The y axis is taken to be horizontal in the magnetic meridional plane and positive southward, whereas the x axis points eastward. Following the formalism developed by Gurevich et al. (1976) for the case when the magnetic field lines in the ionosphere are considered straight lines at inclination I to the y axis, the expression for the square of the length of a line element $ds^2=g_{ik}dx^i dx^k$ takes the form

$$ds^2 = dx^2 + 2\cot I\, dy dz + dy^2 + dz^2/\sin^2 I, \tag{A1}$$

whereas the components of the metric tensor in this nonorthogonal coordinate system become

$$\begin{aligned} &g_{11} = g_{22} = 0,\ g_{33} = 1/\sin^2 I,\\ &g_{12} = g_{21} = g_{13} = g_{31} = 0,\\ &g_{23} = g_{32} = \cot I. \end{aligned} \tag{A2}$$

The conduction current in a plasma is described by means of the conductivity tensor $\hat{\sigma}$, so that

$$\boldsymbol{j} = \hat{\sigma}\boldsymbol{E} = \sigma_0\frac{(\boldsymbol{EB})}{B^2}\boldsymbol{B} + \sigma_P\frac{\boldsymbol{E}B^2 - \boldsymbol{B}(\boldsymbol{EB})}{B^2} + \sigma_H\frac{[\boldsymbol{EB}]}{B},$$

where σ_0, σ_P, σ_H are the longitudinal (parallel to the magnetic field lines), Pedersen and Hall conductivity, respectively. The coordinate transcription of the previous formulae is as follows (Gurevich et al., 1976)

$$\begin{aligned} &j^i = \sigma^{ik}E_k,\\ &\sigma^{ik} = \sigma_0\frac{B^iB^k}{B^2} + \sigma_P\left(g^{ik} - \frac{B^iB^k}{B^2}\right) - \sigma_H\frac{g^{ikl}B_l}{B}, \end{aligned}$$

where g^{ikl} is the antisymmetric fundamental tensor. In the coordinate system adopted in our paper $B^1{=}B^2{=}0$, $B^3{=}1/\sin^2 I$, while for the σ^{ik} components we obtain

$$\begin{aligned} \sigma^{11} &= \sigma_P g_{11},\\ \sigma^{12} &= \sigma_P g_{12} - \sigma_H\sqrt{g_{33}}/\sqrt{g},\\ \sigma^{13} &= \sigma_P g_{13} + \sigma_H\sqrt{g_{23}}/\sqrt{g_{33}g}, \end{aligned} \tag{A3}$$

$$\begin{aligned} \sigma^{22} &= \sigma_P g_{22},\\ \sigma^{23} &= \sigma_P g_{23} - \sigma_H\sqrt{g_{13}}/\sqrt{g_{33}g},\\ \sigma^{33} &= \sigma_0/g_{33} + \sigma_P\,(g_{33} - 1/g_{33}), \end{aligned} \tag{A4}$$

where $g{=}det||g_{ik}||$. The rest of the terms can be calculated by using parity rule, that is, take the σ_P, σ_H coefficients as even and odd, respectively. Finally, using Eqs. (A1), (A3) and (A4) we arrive at the following conductivity tensor

$$\sigma^{ik} = \begin{pmatrix} \sigma_P & -\sigma_H/\sin I & \sigma_H\cos I\\ \sigma_H/\sin I & \sigma_H/\sin^2 I & -\sigma_P\cot I\\ -\sigma_H\cos I & -\sigma_P\cot I & \sigma_0\sin^2 I + \sigma_P\cos^2 I \end{pmatrix}. \tag{A5}$$

Note that this expression now recovers the conductivity elements σ^{13} and σ^{31} that were set to zero in the paper by Shalimov et al. (1998).

To ensure that our final Eqs. (1), (2) from which we start our calculations in the present manuscript are correct, we repeat here their derivation. Using Eq. (A5) we start from the current component flowing out of the layer's top along the magnetic field line (cf. Eq. (3) in the paper by Shalimov et al., 1998):

$$-J^z = \frac{\partial}{\partial x}\left(\Sigma_P^s E_x - \frac{\Sigma_H^s}{S}E_y + \Sigma_H^s C E_z\right) + \frac{\partial}{\partial y}\left(\frac{\Sigma_H^s}{S}E_x + \frac{\Sigma_P^s}{S^2}E_y - \Sigma_P^s C E_z\right), \quad \text{(A6)}$$

where C, S denote $\sin I$, $\cos I$, and the current J^z can be expressed as

$$J^z = -\sigma_H C E_x - \sigma_P \frac{C}{S}E_y + \left(S^2\sigma_0 + C^2\sigma_P\right)E_z. \quad \text{(A7)}$$

Taking into account that $\sigma_0 \gg \sigma_P, \sigma_H$ we can rewrite Eqs. (A6) and (A7) as follows

$$\frac{\partial}{\partial x}\left(\Sigma_P^s E_x - \frac{\Sigma_H^s}{S}E_y\right) - \sigma_H C E_x + \frac{\partial}{\partial y}\left(\frac{\Sigma_H^s}{S}E_x + \frac{\Sigma_P^s}{S^2}E_y\right) - \sigma_P\frac{C}{S}E_y \approx -S^2\sigma_0 E_z. \quad \text{(A8)}$$

Now we make use of the fact that the polarization process results in a curl-free electrostatic field. According to the Stokes theorem, this means that the circulation of the electric field vector along a closed circuit is zero, which also implies that the linear integral between two points is independent of the followed path. Let (1) and (2) be two points of different potential somewhere within a sporadic layer. Then within the layer we have

$$\phi_1 - \phi_2 = \int_1^2 \boldsymbol{E}_\perp^p \cdot d\boldsymbol{l} + \int_1^2 \boldsymbol{E}_\perp^0 \cdot d\boldsymbol{l}_{\rm int} \approx E_x^p l_x^p + E_y^p l_y^p + \int_1^2 \boldsymbol{E}_\perp^0 \cdot d\boldsymbol{l}_{\rm int}, \quad \text{(A9)}$$

where $\boldsymbol{E}_\perp^0$, $d\boldsymbol{l}_{\rm int}$ are the ambient electric field and the path element inside the layer, and l_x^p, l_y^p are the path parts along the x and y direction, respectively. On the other hand, using an external path closure starting from point (1) and going up along the geomagnetic field, then across the geomagnetic field and down along the field line to the point (2), we obtain

$$\phi_1 - \phi_2 = \int_1^2 \boldsymbol{E}_z \cdot d\boldsymbol{l} + \int_1^2 \boldsymbol{E}_\perp^0 \cdot d\boldsymbol{l}_{\rm ext} \approx E_{z1} l_{z1} + E_{z2} l_{z2} + \int_1^2 \boldsymbol{E}_\perp^0 \cdot d\boldsymbol{l}_{\rm ext}, \quad \text{(A10)}$$

where l_{1z}, l_{2z} are the parts of the path along the geomagnetic field outside the layer extended up to a mapping length.

Next, we abandon the rigorous approach and introduce characteristic scale lengths $l_\parallel$ and l_x, l_y for the polarization electric field mapping along the field lines, and the zonal and meridional extents of the layer, respectively. To make easy a comparison with the formalism of Shalimov et al. (1998) (see Eqs. (6) and (7) in their paper), here we also take into consideration the sign of the polarization field, which is positive to the east and negative to the north. Finally, by taking into account that $\int_1^2 \boldsymbol{E}_\perp^0 \cdot d\boldsymbol{l}_{\rm int} \sim \int_1^2 \boldsymbol{E}_\perp^0 \cdot d\boldsymbol{l}_{\rm ext}$, due to almost perfect magnetic field mapping of the ambient electric field we combine the last two equations to obtain $E_x^p l_x - E_y^p l_y \approx (E_{z2} - E_{z1}) l_\parallel$. The right-hand side of the last expression suggests the existence of a potential drop along the field lines which can be approximated by an effective electric field $E_z \approx (E_{z2} - E_{z1})$ so that finally we have

$$E_z l_\parallel \sim E_x^p l_x - E_y^p l_y. \quad \text{(A11)}$$

This relation means that the potential difference $\phi_1 - \phi_2$ inside the layer, and thus the polarization process under consideration, is maintained only through a field-aligned current closure driven by an effective potential drop $E_z l_\parallel$ along and across the geomagnetic field lines. We wish to stress that Eq. (A11) is an approximate and simplified relation, sort of a working hypothesis, which allows for the problem to be treated analytically.

By combining Eqs. (A8) and (A11) we obtain

$$\frac{1}{l_x}\left(\Sigma_P^s E_x - \frac{\Sigma_H^s}{S}E_y\right) - \sigma_H C E_x + \frac{1}{l_y}\left(\frac{\Sigma_H^s}{S}E_x + \frac{\Sigma_P^s}{S^2}E_y\right) - \sigma_P\frac{C}{S}E_y \approx -S^2\sigma_0\frac{E_x^p l_x - E_y^p l_y}{l_\parallel}. \quad \text{(A12)}$$

Further, we note that the total current flow J^z results (see Eqs. (A8), (A12) from two current components associated with the electrostatic fields that set up inside the layer due to the polarization process, the zonal and meridional current flow circuits, respectively. For these two current loops we can write instead of Eq. (A12)

$$\left(\Sigma_P^s E_x - \frac{\Sigma_H^s}{S}E_y\right) - \sigma_H C E_x \approx -S^2\sigma_0\frac{E_x^p l_x^2}{l_\parallel}, \quad \text{(A13)}$$

$$\left(\frac{\Sigma_H^s}{S}E_x + \frac{\Sigma_P^s}{S^2}E_y\right) - \sigma_P\frac{C}{S}E_y \approx S^2\sigma_0\frac{E_y^p l_y^2}{l_\parallel}. \quad \text{(A14)}$$

Note that we can ignore terms with σ_H, σ_P in the left-hand side of Eqs. (A13), (A14) in the following cases: (1) when $C \to 0$ (high-latitude ionosphere), (2) when both, σ_H and σ_P tend to zero (nighttime ionosphere outside sporadic-E), and (3) when both, l_x and l_y are less than $l_\parallel$. The last case follows if one compares terms in the left-hand side of Eqs. (A13), (A14) under the assumption that height-integrated conductances inside and outside a layer are comparable.

Finally, assuming that l_x, l_y are less than $l_\parallel$ and introducing the notations : $R=\Sigma_H^s/\Sigma_P^s$, $Z=\Sigma_P/\Sigma_P^s$, $\Sigma_P=\sigma_P l_\parallel$, $L=l_y/l_x$, $l_\parallel\approx\sqrt{\sigma_0/\sigma_P}/\sqrt{1/l_x^2+1/S^2l_y^2}$ (see here Shalimov et al., 1998, for details) we arrive at Eqs. (6), (7) in the Shalimov et al. (1998) paper and Eqs. (1), (2) in the present manuscript.

Acknowledgements. The completion of this work was made possible with the support of a Greek-Russian collaborative research grant provided jointly by the Greek Secretariat of Research and Technology (GGRT) and the Russian Academy of Sciences. Partial support was also provided by the European Office of Aerospace Research and Development (EOARD), under contract FA8655-03-1-3028 to C. Haldoupis. We wish to thank E. Kudeki who, acting as a reviewer, provided useful suggestions and constructive criticism which helped us improve our paper.

Topical Editor M. Lester thanks two referees for their help in evaluating this paper.

References

Behnke, R. A.: F-layer height bands in nocturnal ionosphere over Arecibo, J. Geophys. Res., 84, 974–978, 1979.

Bourdillon, A., Haldoupis, C., and Delloue, J.: High frequency Doppler radar observations of magnetic aspect sensitive irregularities in the midlatitude E region ionosphere, J. Geophys. Res., 100, 21 503–21 522, 1995.

Bowman, G. G.: Some aspects of mid-latitude spread E_s and its relationships with spread F, Planet Space Sci., 33, 1081–1089, 1985.

Farley, D. T.: A theory of electrostatic fields in a horizontally stratified ionosphere subject to a vertical magnetic field, J. Geophys. Res., 64, 1225–1235, 1959.

Fukao, S., Shirakawa, T., Takami, T., Yamamoto, M., Tsuda, T., and Kelley, M.C.: Turbulent upwelling of the mid-latitude ionosphere. 1. Observational results by the MU radar, J. Geophys. Res., 96, 3725–3746, 1991.

Fukao, S., Yamamoto, M., Tsunoda, R. T., Hayakawa, H., and Mukai, T.: The SEEK (Sporadic E Experiment over Kyushu) campaign, Geophys. Res. Lett., 25, 1761–1764, 1998.

Garcia, F. J., Kelley, M. C., Makela, J. J., and Huang, C.-S.: Airglow observations of mesoscale low-velocity travelling ionospheric disturbances at midlatitudes, J. Geophys. Res., 105, 18 407–18 415, 2000.

Gurevich, A. V., Krylov, A. L., and Tsedilina, E. E.: Electric fields in the Earths's magnetosphere and ionosphere, Space Sci. Rev., 19, 59–251, 1976.

Haldoupis, C. and Schlegel, K.: A 50-MHz radio Doppler experiment for midlatitude E region coherent studies: System description and first results, Radio Sci., 28, 959–978, 1993.

Haldoupis, C., Schlegel, K., and Farley, D. T.: An explanation for type 1 echoes radar echoes from the midlatitude E region ionosphere, Geophys. Res. Lett., 23, 97–100, 1996.

Haldoupis, C., Farley, D. T., and Schlegel, K.: Type 1 radar echoes from the midlatitude E region, Ann. Geophys., 28, 908–917, 1997.

Haldoupis, C., Hussey, G. C., Bourdillon, A., and Delloue, J.: Azimuth-Time-Intensity striations of quasiperiodic radar echoes from the midlatitude E region ionosphere, Geophys. Res. Lett., 28, 1933–1937, 2001.

Haldoupis, C., Kelley, M. C., Hussey, G. C., and Shalimov, S.: Role of unstable sporadic-E layers in the generation of midlatitude spread-F, J. Geophys. Res., 108, doi:10.1029/2003JA009956, 2003.

Harper, R. M. and Walker, J. C. G.: Comparison of electrical conductivities in the E- and F-regions of the nocturnal ionosphere, Planet. Space Sci., 25, 197–198, 1977.

Hussey, G. C., Schlegel, K., and Haldoupis, C.: Simultaneous 50 MHz coherent backscatter and digital ionosonde observations in the mid-latitude E-region, J. Geophys. Res., 103, 6991–7002, 1998.

Hysell, D. L. and Burcham, J. D.: The 30-MHz radar interferometer studies of mid-latitude E-region irregularities, J. Geophys. Res., 105, 12 707–12 812, 2000.

Hysell, D. L., Yamamoto, M., and Fukao, S.: Simulations of plasma clouds in the midlatitude E region ionosphere with implications for type 1 and type 2 echoes, J. Geophys. Res., 107(A10), SIA 17–1, doi:10.1029/2002JA009291, 2002.

Hysell, D. L., Larsen, M. F., and Zhou, Q. H.: Common volume coherent and incoherent scatter radar observations of midlatitude sporadic E layers and QP echoes, Ann. Geophys., 22, 3277–3290, 2004,
SRef-ID: 1432-0576/ag/2004-22-3277.

Kelley, M. C.: The Earth's Ionosphere: Plasma Physics and Electrodynamics, Academic, San Diego, Calif., 1989.

Kelley, M. C., Makela, J. J., Swartz, W. E., Collins, S. C., Thonnard, S., Aponte, N., and Tepley, C.A.: Caribbean Ionospheric campaign, year one: Airglow and plasma conditions during two intense mid-latitude spread-F events, Geophys. Res. Lett., 27, 2825–2829, 2000.

Kelley, M. C. and Makela, J. J.: Resolution of the discrepancy between experiment and theory of midlatitude F region structures, Geophys. Res. Lett., 28, 2589–2592, 2001.

Kelley, M. C., Haldoupis, C., Nicolls, M. J.,Makela, J. J., Belehaki, A., Shalimov, S., and Wong, V. K.: Case studies of coupling between the E and F regions during unstable sporadic-E conditions, J. Geophys. Res., 108, doi:10.1029/2003JA009955, 2003.

LaBelle, J.: Mapping of electric field structures from the equatorial E region to the underlying E region, J. Geophys. Res., 90, 4341–4346, 1985.

Larsen, M. F.: Winds and shears in the mesosphere and lower thermosphere: results from four decades of chemical release wind measurements, J. Geophys. Res., 107, doi10.1029/2001JA000218, 2002.

Mendillo, M., Baumgardner, J., Nottingham, D., Aarons, J., Reinisch, B., Scali, J., and Kelley, M. C.: Investigations of thermospheric-ionospheric dynamics with 6300 A images from the Arecibo Observatory, J. Geophys. Res., 102, 7331–7344, 1997.

Ogawa, T., Takahashi, O., Otsuka, Y., Nozaki, K., Yamamoto, M., and Kita, K.: Simultaneous middle and upper atmosphere radar and ionospheric sounder observations of midlatitude E region irregularities and sporadic E layer, J. Geophys. Res., 107, 1275, doi:10.1029/2001JA900176, 2002.

Riggin, D., Swartz, W. E., Providakes, J., and Farley, D. T.: Radar studies of long-wavelength waves associated with mid-latitude sporadic-E layers, J. Geophys. Res., 91, 8011–8024, 1986.

Schlegel, K. and Haldoupis, C.: Observation of the modified two-stream plasma instability in the mid-latitude E region ionosphere, J. Geophys. Res., 99, 6219–6226, 1994.

Shalimov, S., Haldoupis, C., and Schlegel, K.: Large polarization electric fields associated with midlatitude sporadic E, J. Geo-

phys. Res., 103, 11 617–11 625, 1998.

Shiokawa, K., Ihara, C., Otsuka, Y., and Ogawa, T.: Statistical study of nighttime medium-size travelling ionospheric disturbances using midlatitude airglow images, J. Geophys. Res., 108, A1, SIA 13-1, doi10.1029/2002JA009492, 2003.

Swartz, W. E., Collins, S. C., Kelley, M. C., Makela, J.J., Kudeki, E., Franke, S., Urbina, J., Aponte, N., Gonzalez, S., Siltzer, M. P., and Friedman, J. S.: First observations of F region upwelling coincident with severe E region plasma and neutral atmosphere perturbations, J. Atmos. Sol.-Terr. Phys., 64, 1545–1556, 2002.

Tsunoda, R. T. and Cosgrove, R. B.: Coupled electrodynamics in the nighttime midlatitude ionosphere, Geophys. Res. Lett., 28, 4171–4174, 2001.

Tsunoda, R. T., Cosgrove, R. B., and Ogawa, T.: Azimuth-dependence E_s layer instability: A missing link, J. Geophys. Res., 109(A12), doi:10.1029/2004JA010597, 2004.

Yamamoto, M., Fukao, S., Ogawa, T., Tsuda, T., and Kato, S.: A morphological study of mid-latitude E region field-aligned irregularities observed with the MU radar, J. Atmos. Terr. Phys., 54, 769–777, 1992.

Yokoyama, T., Yamamoto, M., and Fukao, S.: Computer simulation of polarization electric fields as a source of midlatitude field-aligned irregularities, J. Geophys. Res., 108, A2, SIA 2–1, doi:10.1029/2002JA009513, 2003.

Yokoyama, T., Yamamoto, M., Fukao, S., and Cosgrove, R. B.: Three-dimensional simulation on generation of polarization electric field in the midlatitude E-region ionosphere, J. Geophys. Res., 109(A1), A01309, doi: 10.1029/2003JA010238, 2004.